ACS OMEGA

Open Access

http://pubs.acs.org/journal/acsodf

Article

Study on the Impact of Porous Media on Condensate Gas Depletion: A Case Study of Reservoir in Xihu Sag

Hengjie Liao, Xianke He, Ping Guo,* Shuoshi Wang,* Yuansheng Li, Zhehao Jiang, Limiao Wang, Ruifeng Xu, and Hanmin Tu

Cite This: *ACS Omega* 2024, 9, 43850−43863

Read Online

ACCESS | Metrics & More | Article Recommendations

ABSTRACT: During the depletion and pressure reduction process in condensate gas reservoirs, the precipitation of condensate oil transforms the single-phase gas flow into a two-phase gas−liquid flow, significantly reducing the permeability. Currently, microscopic studies of the phase behavior of condensate gas in porous media mainly focus on observing and describing the occurrence of condensate oil, lacking quantitative calculations and direct observations of condensate oil throughout the entire depletion cycle. This paper uses a microvisualization method to simulate the depletion process of condensate gas reservoirs. Condensate gases with oil contents of 175.3 and 505.5 g/cm^3 were prepared by mixing methane, ethane, hexane, and decane in specific proportions. Pore structures were extracted from thin sections of real core casts, and microfluidic chips with a minimum pore diameter of 20 μm and an areal porosity of 20.75% were fabricated by using a chemical wet etching method. Subsequently, microfluidic condensate gas depletion experiments were conducted with chip images recorded during the depletion process. Grayscale analysis of the depletion images was performed using ImageJ software to quantitatively calculate condensate oil saturation and recovery rates, analyzing the effects of different condensate oil contents on condensate gas depletion, and comparing the differences between depletion in porous media and in a PVT cell. The conclusions drawn are as follows: the dew points of high and low in the porous media are 3.15% and 1.85% higher than those in the PVT cell, respectively. In the early stages of depletion, condensate oil saturation in porous media is higher than that in the PVT cell, while in the middle to late stages, condensate oil saturation in porous media is lower than that in the PVT cell. The condensate oil recovery rate in porous media is significantly higher than the depletion recovery rate in the PVT cell. Condensate oil tends to precipitate and disperse at blind ends and corners, while it easily forms patches in mainstream large pores.

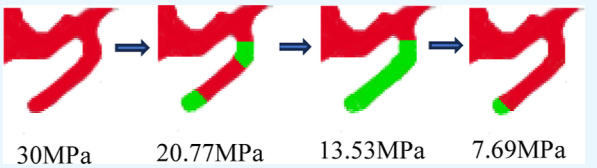

1. INTRODUCTION

Compared with conventional oil and gas reservoirs, condensate gas reservoirs have a unique retrograde condensation phenomenon. During development, once the formation pressure falls below the dew point pressure of the condensate gas reservoir, the condensate gas, originally existing as a single gas phase underground, undergoes retrograde condensation. The heavy components in the condensate gas separate out in a liquid form, resulting in the coexistence of gas and liquid phases in the formation,[1−3] leading to a decrease in the relative permeability of the gas phase in the reservoir,[4−7] ultimately reducing the recovery of condensate oil and gas, and causing a waste of valuable resource.[8] Condensate oil and gas are commonly found in carbonate, sandstone, and shale reservoirs. Therefore, to effectively develop condensate gas reservoirs, it is crucial to analyze the phase behavior of condensate gas at micro- and nanoscales.[9,10]

Conventional condensate gas phase behavior experiments mostly use PVT cells. Sui[11] conducted depletion studies of the condensate oil−gas system with and without porous media using PVT cells and long core experiments, showing that there are significant differences between the phase behavior of the condensate oil−gas system in porous media and the conventional PVT cells, indicating that PVT cells cannot truly reflect the phase behavior changes of condensate oil−gas in the porous media.[12] Guo[13] used carbonate cores with artificially created vugs and fractures to study the depletion of condensate gas with a high condensate oil content, and the results showed that the presence of porous media enhanced the recovery of condensate oil. Core experiments simulate condensate gas depletion by monitoring the composition changes of the effluent gas to reflect the phase behavior. The retrograde condensate oil saturation in the core is inferred indirectly from the analysis of effluent. The flowthrough experiment cannot directly observe the phase behavior of condensate gas, and the experiment is time-

Received: July 26, 2024
Revised: October 4, 2024
Accepted: October 11, 2024
Published: October 19, 2024

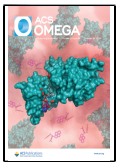

https://doi.org/10.1021/acsomega.4c06866
ACS Omega 2024, 9, 43850−43863

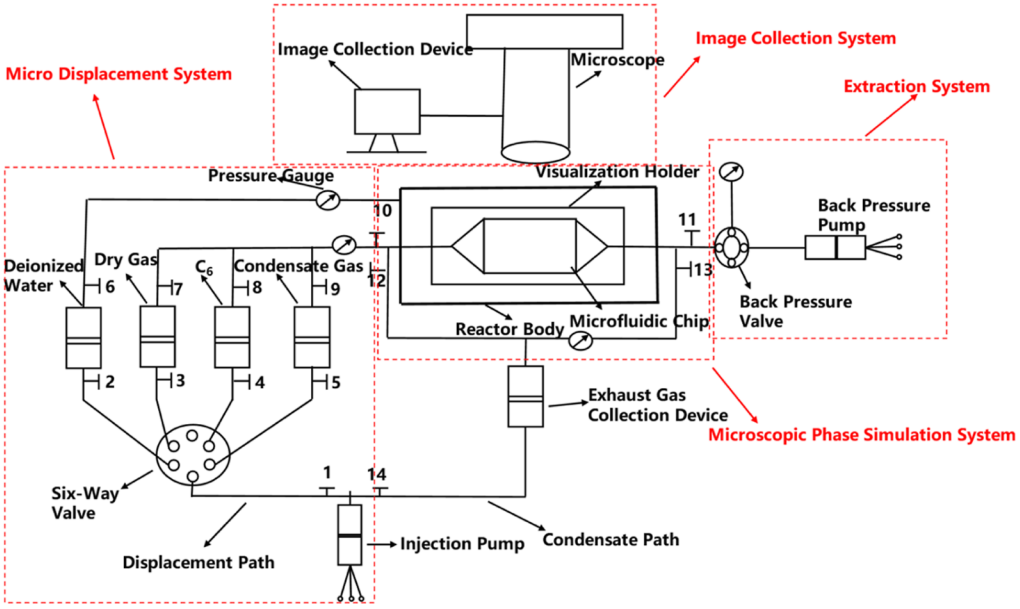

Figure 1. High-temperature high-pressure microfluidic condensate gas depletion experimental flowchart (1−14 are valves).

consuming.[14−18] Li et al. used real cores and conducted core flooding and chromatographic analysis to study the impact of the condensate oil flow on condensate oil saturation. However, their approach makes it difficult to observe the actual phase behavior changes of the condensate gas.[19] Currently, there is a lack of experimental methods that could directly study the impact of the porous media on the phase behavior of condensate oil and gas and observe the phase behavior of condensate gas in porous media.

In recent years, with the development of various microfluidic device manufacturing technologies and image acquisition and processing technologies, microfluidic methods that accurately control fluid flow behavior in micronano channels have emerged.[20] Compared with traditional physical simulation experiments, they have the advantages of real-time visualization, small sample consumption, and short measurement time.[21] Their visualization advantages can also help researchers better understand fluid dynamics on the pore scale of rocks.

Wang and Li established a microscopic experimental method for phase behavior in porous media, using a two-dimensional micro model and a three-dimensional micro model to study the condensate gas and concluded that porous media aggravates the occurrence of retrograde condensation.[22] Zhu directly observed the flow characteristics of condensate oil using a microscopic visual glass model, studied the migration mechanism and flow patterns of condensate oil and gas, and explained the deposition and migration rules of wax and the phase change and transport rules of condensate oil−gas−solid.[23]

Yang and Zhong et al. used standardized nanoscale chips to study the phase behavior of condensate gas, but their chips do not possess the complex pore structures of porous media.[24,25] Jing et al., while using micro- and nanoscale chips to observe the phase behavior characteristics of condensate gas and quantitatively measure the saturation of condensate oil in porous media, did not account for the impact of condensate oil flow on the experimental results.[26]

There are limited research results on the condensate gas phase or flow based on microfluidic technology. Research on the phase behavior in porous media mainly focuses on the observation and description of condensate oil occurrence, lacking quantitative calculations of condensate oil throughout the depletion cycle. Quantitative research results on phase behavior are based on standardized microfluidic models without considering the pore structure of the reservoir. This paper prepared a microfluidic chip based on thin sections of real core from the Xihu Sag, which simulated the depletion process of condensate gas reservoirs, and quantitatively calculated the recovery rates of condensate gas and oil. Meanwhile, the formation, distribution, and microscopic flow mechanism of condensate oil and gas were studied in depth. Finally, an in-depth analysis was conducted on the depletion results of condensate gas in microfluidic chip porous media and its PVT cell.

2. MICROFLUIDIC CONDENSATE GAS DEPLETION EXPERIMENT DESIGN

2.1. Experimental Equipment. In microfluidic experiments, the dead volume in the pipelines is generally at the microliter level, while the fluid required for microfluidic experiments is usually at the microliter level. Therefore, eliminating the impact of the dead volume is key to the success of this experiment. Unlike conventional single-direction pressure depletion experiments for condensate gases, this study innovatively developed a microfluidic bidirectional pressure depletion method. This method allows fluid to flow outward simultaneously from both ends of the chip, ensuring that the fluid in the dead volume of the pipelines never enters the chip, thereby eliminating the impact of the dead volume on the accuracy of the experiment.

The device includes a microdisplacement system, a microfluidic chip holding system, a microscopic image acquisition system, and a production system, with the experimental flowchart, as shown in Figure 1.

The microdisplacement system is mainly responsible for controlling the internal pressure, confining pressure, and back pressure of the microfluidic chip. It mainly includes a microdisplacement pump, a sample container filled with condensate gas, a six-way valve, a back pressure pump, an intermediate container filled with hexane, an intermediate

https://doi.org/10.1021/acsomega.4c06866
ACS Omega 2024, 9, 43850−43863

container filled with dry gas, an intermediate container filled with deionized water, and an intermediate container for collecting waste gas.

The main device of the microfluidic chip holding system is the high-temperature and high-pressure view cell, which consists of end-caps with sapphire observation glasses and a cell body. The middle of the cell is a chip holding device, which fixes the chip onto the holder by using threaded stainless-steel screws and rubber gaskets, as shown in Figure 2.

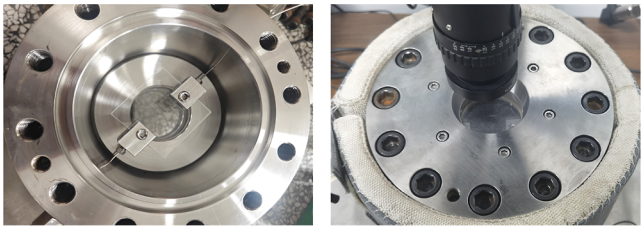

Internal of the Reactor Body Exterior of the Reactor Body

Figure 2. High-temperature high-pressure visualization holder.

A microscopic image acquisition system consists of a Leica Z16APO microscope, a Leica Flexacam C1 camera, and image processing software LAS X. A Leica Z16APO microscope has a zoom ratio of 16:1, with a magnification range of 7.1−575×, and includes a fixed magnification slot to ensure repeatable observations at specific magnifications, facilitating repeat experiments. The Leica Flexacam C1 camera's built-in Auto Scale function can automatically adjust the grayscale of real-time images, creating a strong contrast between bright condensate oil and condensate gas upon precipitation. These images can be used to quantitatively study the condensate oil saturation throughout the depletion cycle in a microfluidic model. The microscope is equipped with an adjustable intensity external light source at the bottom to ensure image clarity, as shown in Figure 3.

The production system mainly consists of a back pressure pump and a back pressure valve, which is used to adjust the system's back pressure to control the fluid at the outlet end.

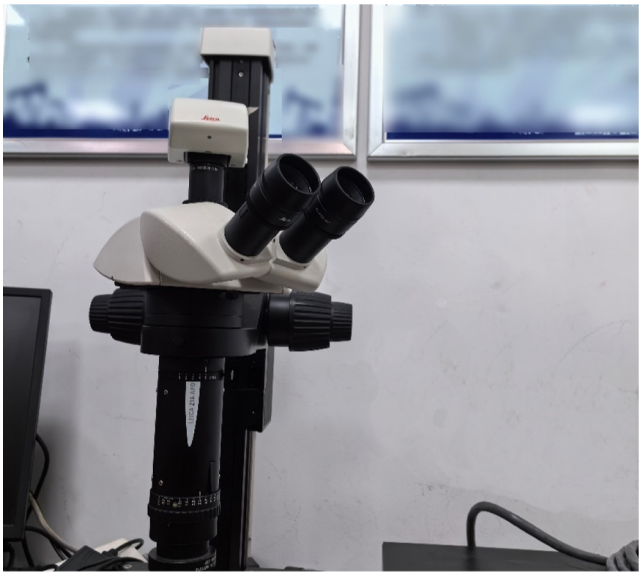

Figure 3. Microscopic image acquisition system.

2.2. Experimental Materials. *2.2.1. Porous Media.* The porous media in this study are microfluidic chips, and the design and manufacturing process steps are as follows:

(1) Extract the pore structure from thin sections of real core castings using CAD software in equal proportions, as shown in Figure 4A,B.

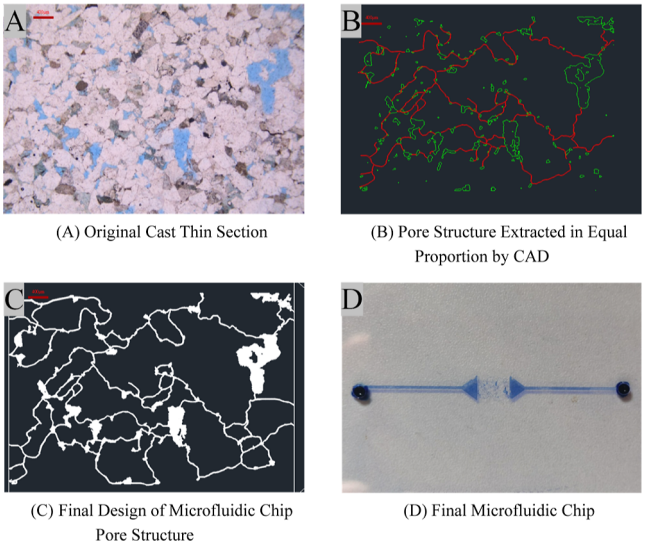

(A) Original Cast Thin Section (B) Pore Structure Extracted in Equal Proportion by CAD

(C) Final Design of Microfluidic Chip Pore Structure (D) Final Microfluidic Chip

Figure 4. Design and preparation process of microfluidic chip.

(2) Process the extracted pore structure by connecting isolated large pores and removing isolated small pores. The minimum line width for fabrication is 20 μm, so isolated small pores smaller than 20 μm were removed, and the remaining isolated pores are connected by throats, as shown in Figure 4B,C.

(3) Prepare the microfluidic chip using chemical wet etching. The chip material is B270 glass (a modified glass composed of silica, calcium oxide, sodium oxide, etc.). It is water-wet, has high transparency, chemical resistance, and high-temperature resistance. The chip has a minimum pore size of 20 μm, a maximum pore size of 330 μm, and an areal porosity of 20.75%, providing sufficient space for condensate oil to condense. The overall structure of the chip is a square with a side length of 6.3 cm. The final microfluidic chip is shown in Figure 4D.

2.2.2. Experimental Fluids. The CMG-Winprop module is used to predict the single stage flash and constant volume depletion experiment for simulated condensate gas under experimental conditions of 70 °C and 30 MPa. The predicted simulated condensate gas sample's single gas oil ratio (GOR) and maximum retrograde condensate liquid volume are close to the PVT report of the real fluid sample. The compositions and main parameters of two condensate gas samples with different condensate oil contents are shown in Table 1.

According to the predicted condensate gas formulation, the simulated condensate gas sample was prepared according to the national standard GB/T26981-2020 "Analysis Methods for Fluid Properties in Oil and Gas Reservoirs" to provide experimental fluid for subsequent microscopic experiments.

The sample preparation results for the two types of condensate gases with different condensate oil contents are shown in Table 2.

https://doi.org/10.1021/acsomega.4c06866
ACS Omega 2024, 9, 43850−43863

Table 1. Compositions and Main Parameters of Condensate with Two Different Condensate Oil Contents

condensate oil content	gas phase composition	oil phase composition	predicted gas−oil ratio (m^3/m^3)	predicted maximum retrograde condensate liquid volume (%)
high condensate oil content	46.5% methane, 46.5% ethane	7% decane	1814	22.53
low condensate oil content	48% methane, 48% ethane	1.2% hexane + 2.8% decane	4778	6.36

Table 2. Predicted Results and Actual Preparation Results for Condensate Gas with Two Different Condensate Oil Contents

parameter	low		high	
	actual results	predicted results	actual results	predicted results
reservoir temperature, °C	70	70	70	70
reservoir pressure, MPa	30	30	30	30
gas−oil ratio (GOR), m^3/m^3	4062	4778	1454	1814
dew point pressure, MPa	20.34	15.60	21.03	18.90
maximum retrograde liquid, %	7.97	6.37	24.30	22.53

Flash vaporization compositions for two types of condensate gas with different condensate oil contents are shown in Table 3.

Table 3. Flash Vaporization Compositions for Two Types of Condensate Gas with Different Condensate Oil Contents

composition	low		high	
	flashed oil (mol %)	flashed gas (mol %)	flashed oil (mol %)	flashed gas (mol %)
methane		47.40		47.22
ethane		52.60		52.78
hexane	31.11			
decane	68.89		100.00	
Σ total	100.00	100.00	100.00	100.00

2.3. Experimental Methods and Procedures. *2.3.1. Microfluidic Condensate Gas Depletion Experimental Method.* A microvisualization chip was prepared based on the thin sections of cores from the Xihu Sag to conduct an in-depth study on the formation, aggregation, distribution of condensate oil, and the microscopic flow mechanism of condensate oil and gas during depletion. The experimental temperature is 70 °C, and the experimental pressure is 30 MPa. The microfluidic condensate gas depletion experimental procedure is as follows:

1 Load the prepared microfluidic chip into the microfluidic chip holder and evacuate the microfluidic chip.
2 Add enough deionized water to the view cell and maintain the temperature of the cell at 70 °C.
3 Inject hexane to increase the internal pressure of the microfluidic model, synchronize the confining pressure and internal pressure to the experimental pressure (30 MPa) and continuously apply a back pressure 1−2 MPa higher than the confining and internal pressures during this process.
4 After reaching the experimental pressure, begin displacing C6 with dry gas while maintaining the confining and internal pressures at 30 MPa. Continue displacement up to 10,000 PV.
5 Connect the condensate gas container, displace approximately 10,000 PV of condensate gas into the microfluidic model at a back pressure of 30 MPa using a flow rate of 0.03 mL/min to replace the dry gas.
6 Close the valves of the displacement path, open the depletion path (synchronous depletion) valves, and use the pump to simultaneously reduce the confining and internal pressures in the step-wise manner to conduct the depletion experiment. Transfer the depleted waste liquid to the waste liquid accumulator. Use the image acquisition system to capture images of the microfluidic condensate gas depletion process to observe the phase behavior and distribution of condensate oil and gas.

2.3.2. Microfluidic Condensate Oil Saturation Calculation Method. To quantitatively calculate the saturation and recovery rate from microscopic images, ImageJ is used for image processing. The calculation of condensate oil saturation and recovery rate can be based only on the images captured by the camera. When the white condensate oil precipitates, it forms a sharp contrast with the gray condensate gas. By differentiation of the white condensate oil and gray condensate gas and using ImageJ for pixel statistics, the condensate oil saturation and recovery can be calculated. This method avoids errors from effluent collection and achieves quantitative analysis of the fluids within the microfluidic model.

1. Process the experimental image after gas saturation (as shown in Figure 5a). Use the color-processed saturated gas image (as shown in Figure 5b) as Template 1. Convert the image to 8 bit, then use the ImageJ image-adjust-threshold function to adjust the grayscale to an appropriate value. After adjustment, use the software's analysis function to calculate the percentage of the red area (void area) in the entire image.
2. Process the image to define the pore wall (as shown in Figure 5c). Using the same method as in step (1), calculate the pixel percentage occupied by the channel wall. Subtract the pixel percentage occupied by the channel wall from the percentage of gas and channel wall calculated in step (1), which gives the actual pixel percentage occupied by the gas. This percentage is defined as porosity φ.
3. Import the image at a certain pressure point into ImageJ software. Using the same method as in step (1), calculate the pixel percentage occupied at this time (as shown in Figure 5d). Subtract the pixel percentage occupied at this time (as shown in Figure 5d) from the gas and channel wall percentage calculated in step (1) (as shown in Figure 5b). The reduced part is the percentage of precipitated condensate oil, defined as a.
4. Condensate oil saturation $S_o = \frac{a}{\varphi}$.

2.3.3. Microfluidic Condensate Gas Recovery Calculation Method. To calculate the recovery rate of condensate oil, the amount of condensate oil recovered must be measured. Due to the extremely small quantities in microscopic experiments,

https://doi.org/10.1021/acsomega.4c06866
ACS Omega 2024, 9, 43850−43863

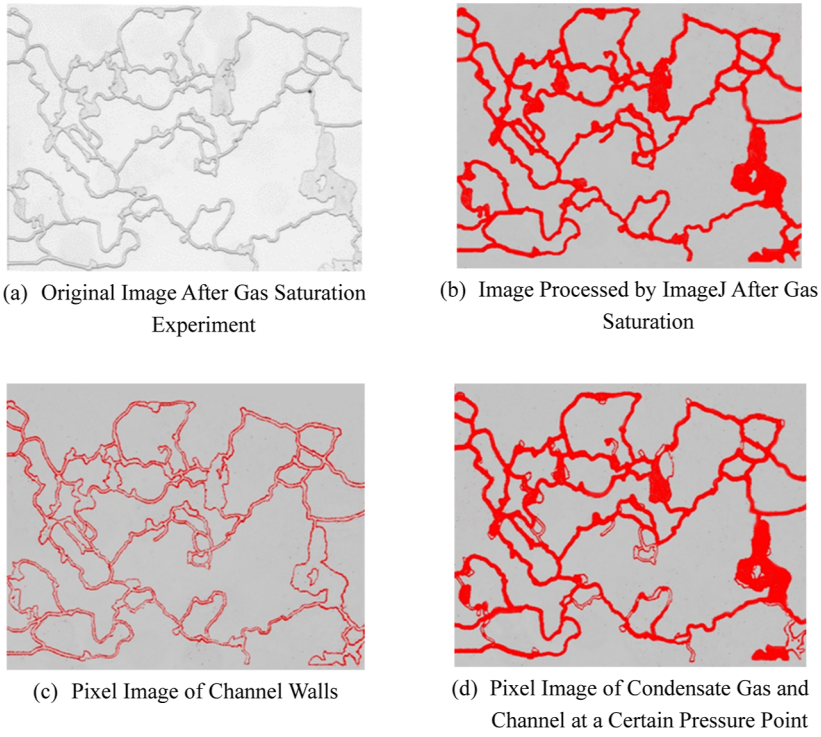

Figure 5. Calculation of condensate oil saturation using ImageJ software.

direct measurement is difficult, so we must start with the amount of oil remaining in the chip. The oil remaining in the chip consists of two parts: one part precipitates directly in the chip as a condensate oil, and the other part remains in the chip as a gas phase without precipitating. The total amount of unrecovered oil is the sum of these two parts, which can then be used to calculate the recovery rate of the condensate oil.

The condensate oil precipitated in the chip could be directly measured through image pixels. The part of the oil that remains in the gas phase without precipitating can be calculated using the gas−oil ratio parameters obtained from the constant volume depletion experiment by back-calculating the condensate oil content in the gas phase. Below is the detailed process for calculating the condensate oil recovery rate.

(i) Use a vernier caliper to accurately measure the length and width of the etched area of the microfluidic chip to obtain the etched area A. According to the etching depth h and the surface porosity φ of the microfluidic chip (image pixels of the microfluidic chip not saturated with any fluid), calculate the pore volume V_P of the microfluidic chip using Formula 1, and calculate the corresponding gas storage volume V_g of the microfluidic chip using Formula 2

$$V_P = Ah\varphi \tag{1}$$

$$V_g = Ah\varphi S_g \tag{2}$$

In the formulas: V_P—pore volume of the microfluidic chip, cm^3; V_g—gas storage volume corresponding to the microfluidic chip, cm^3; A—etched area, cm^2; h—etching depth, μm; φ—surface porosity of the microfluidic chip, %; and S_g—Condensate gas saturation, %;

(ii) Using a condensate gas-saturated microfluidic chip, where the condensate gas saturation S_g is 1, calculate the gas storage volume $V_{g\text{-initial}}$ corresponding to the initial state of the microfluidic chip using Formula 2. According to the condensate gas sample preparation report, obtain the initial gas−oil ratio $GOR_{initial}$ and the initial condensate gas volume factor $B_{g\text{-initial}}$. Calculate the total amount of condensate oil $V_{O\text{-initial}}$: in the initial state of the microfluidic chip

$$V_{sc\text{-initial}} = \frac{V_{g\text{-initial}}}{B_{g\text{-initial}}} \tag{3}$$

$$V_{O\text{-initial}} = \frac{V_{sc\text{-initial}}}{GOR_{initial}} \tag{4}$$

In the formulas: $V_{g\text{-initial}}$—gas storage volume corresponding to the initial state (Sg = 1S_g = 1Sg = 1) of the microfluidic chip, cm^3; $V_{sc\text{-initial}}$—volume of condensate gas in the initial state at standard conditions, cm^3; $B_{g\text{-initial}}$—initial condensate gas volume factor, dimensionless; $GOR_{initial}$—initial gas−oil ratio, m^3/m^3; and $V_{O\text{-initial}}$—total amount of condensate oil in the initial state of the microfluidic chip, mL;

(iii) Conduct the depletion experiment according to the predetermined pressure steps, stopping when the pressure drops to the target pressure point P below the dew point pressure.

(iv) To calculate the total amount of condensate oil within the microfluidic chip, including the precipitated condensate oil and the condensate oil that has not precipitated from the condensate gas within the chip, follow these steps:

(1) Calculate the amount of precipitated condensate oil within the microfluidic chip: import the image of the microfluidic chip, which contains the precipitated condensate oil at a pressure below the dew point, was imported into the image processing software. Select an appropriate grayscale range; the high-grayscale part represents the condensate gas.

https://doi.org/10.1021/acsomega.4c06866
ACS Omega 2024, 9, 43850−43863

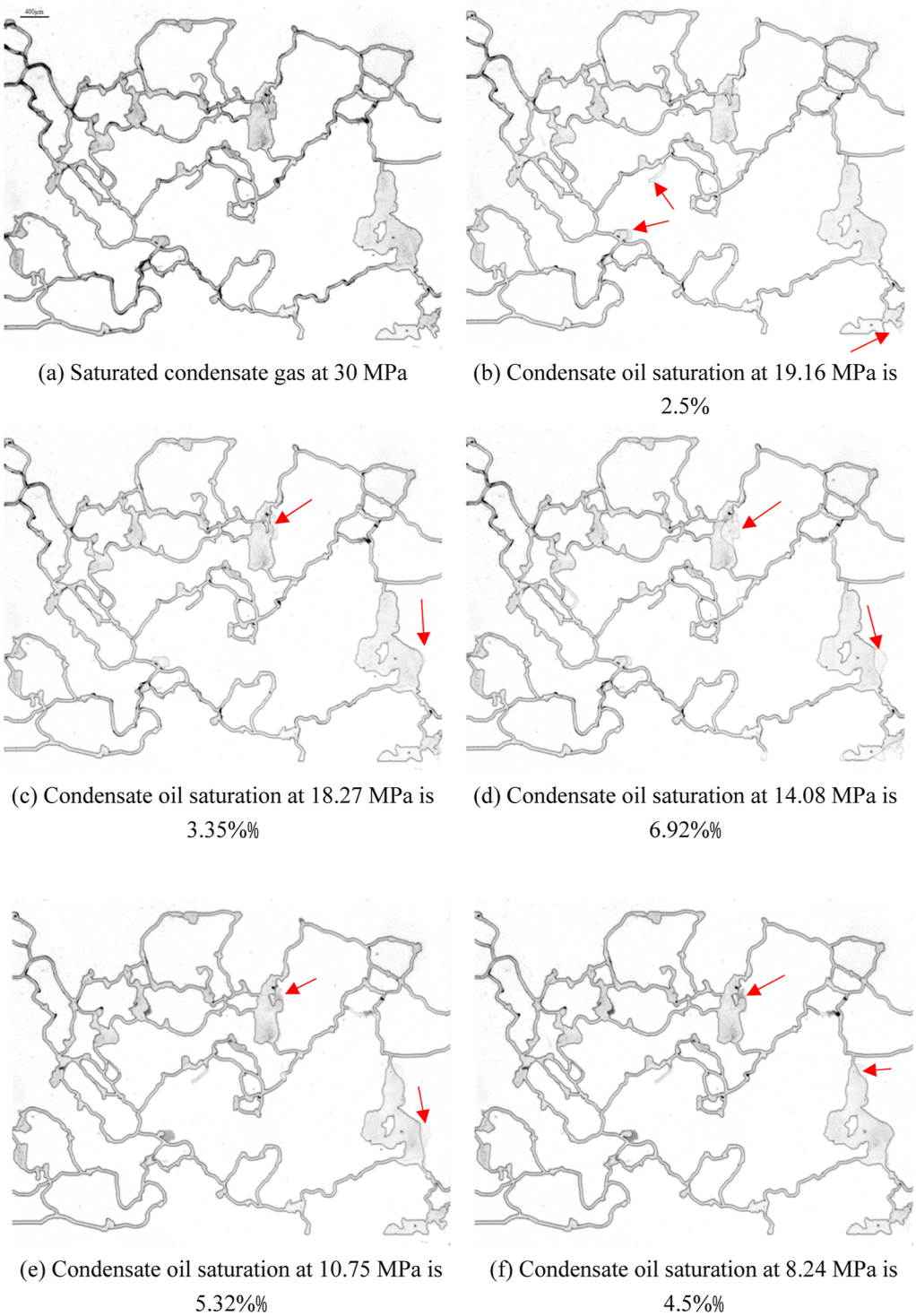

Figure 6. Microscale depletion experiment images of low condensate oil content gas.

Calculate the percentage of pixels corresponding to the current condensate gas. Subtract the percentage of pixels corresponding to the current condensate gas from the area porosity to obtain the percentage of the condensate oil. This gives the current condensate oil saturation S_o and condensate gas saturation S_g within the microfluidic chip. Calculate the amount of precipitated condensate oil V_{po1} within the microfluidic chip using Formula 5

$$V_{po1} = V_P \times S_o \tag{5}$$

In the formula: V_{po1}—amount of precipitated condensate oil within the microfluidic chip, ml; V_P—pore volume of the microfluidic chip, cm^3; S_o—condensate oil saturation within the microfluidic chip, %. Convert V_{po1} to the amount of precipitated condensate oil within the microfluidic chip at standard surface conditions V_{o1}.

https://doi.org/10.1021/acsomega.4c06866
ACS Omega 2024, 9, 43850−43863

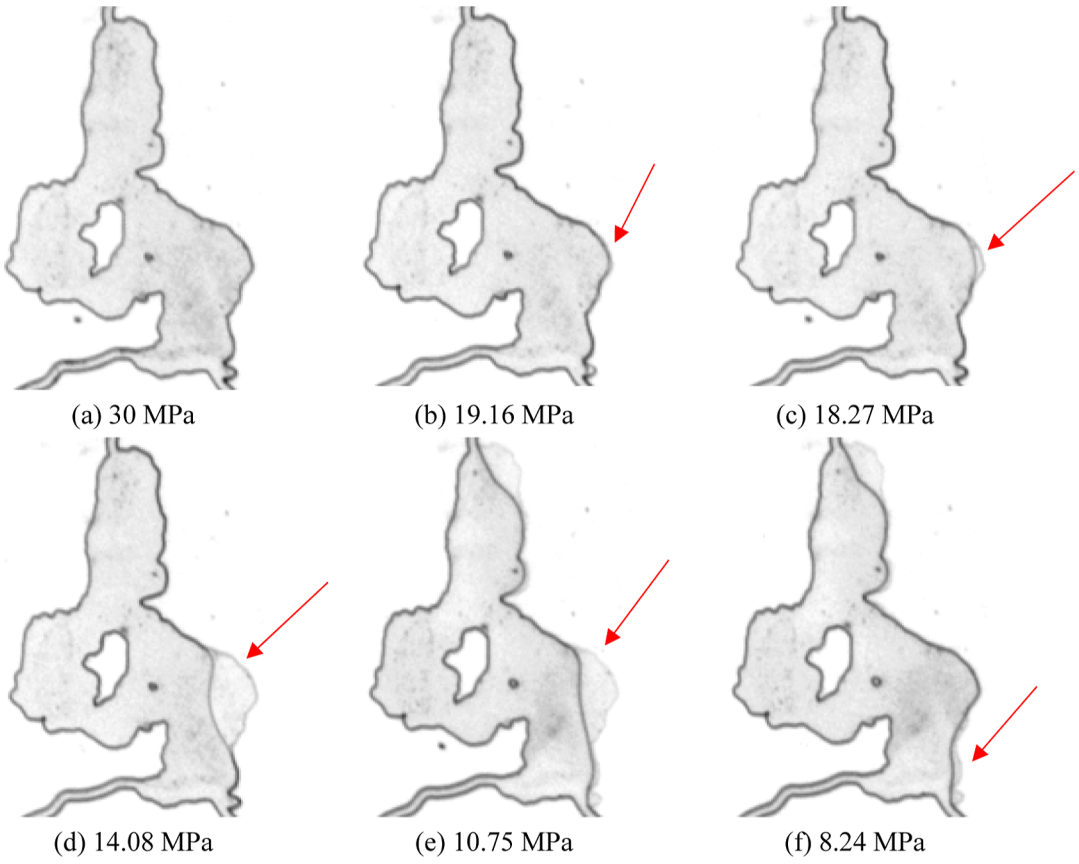

Figure 7. Condensate oil phase change in the main large pore during depletion.

$$V_{o1} = \frac{V_{po1}}{c} \tag{6}$$

In the formula: V_{o1}—amount of precipitated condensate oil within the microfluidic chip at standard surface conditions, mL; and c—condensate oil volume correction factor, dimensionless;

(2) Calculate the amount of condensate oil in the microfluidic chip that has not precipitated from the condensate gas: conduct a constant volume depletion experiment on the condensate gas to obtain the condensate gas and condensate oil at the target pressure point P and determine the depletion gas−oil ratio (GOR) and condensate oil content σ. Measure the composition of the condensate gas using a gas chromatograph to obtain the condensate gas density ρ_g at standard surface conditions and ρ_{gf} under formation conditions. Measure the composition of the condensate oil using an oil chromatograph to obtain the condensate oil density ρ_c. Calculate the condensate gas volume factor B_g using Formula 7

$$B_g = \frac{\rho_g + 10^{-6}\sigma\rho_c}{\rho_{gf}} \tag{7}$$

In the formula: substitute the current gas saturation S_g of the microfluidic chip into Formula 2 to calculate the gas storage volume V_g corresponding to the microfluidic chip. Then, the volume of condensate gas at standard surface conditions V_{sc} within the microfluidic chip was calculated using Formula 8

$$V_{sc} = \frac{V_g}{B_g} \tag{8}$$

In the formula: B_g—condensate gas volume factor, dimensionless; V_{sc}—volume of condensate gas at standard surface conditions within the microfluidic chip, cm^3; calculate the amount of condensate oil that has not precipitated from the condensate gas within the microfluidic chip V_{o2} using Formula 9

$$V_{o2} = \frac{V_{sc}}{GOR} \tag{9}$$

In the formula: V_{o2}—amount of condensate oil that has not precipitated from the condensate gas within the microfluidic chip, mL; and GOR—depletion gas−oil ratio, m^3/m^3;

(5) Calculate the total amount of condensate oil $V_{o\text{-total}}$ within the microfluidic chip, then use the initial total amount of condensate oil $V_{O\text{-initial}}$ in the microfluidic chip to calculate the condensate oil recovery rate E for the microfluidic experiment

$$V_{o\text{-total}} = V_{o1} + V_{o2} \tag{10}$$

$$E = \left(1 - \frac{V_{o\text{-total}}}{V_{o\text{-initial}}}\right) \times 100 \tag{11}$$

In the formula: E—condensate oil recovery rate, %.

https://doi.org/10.1021/acsomega.4c06866
ACS Omega 2024, 9, 43850−43863

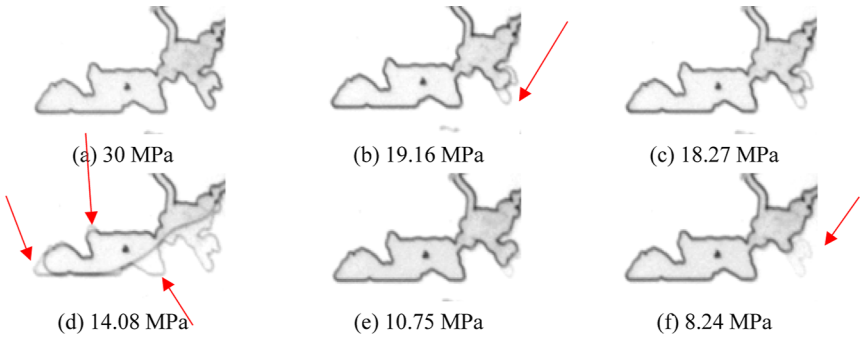

Figure 8. Condensate oil phase change in a pore not located in the main flow channel during depletion.

3. EXPERIMENTAL RESULTS AND ANALYSIS

3.1. Microscopic Depletion Experiment of Low Condensate Oil Content Condensate Gas. *3.1.1. Visualization Characterization of Microscopic Occurrence.* The entire microscale depletion experiment for low condensate oil content gas is shown in Figure 6, where the gray areas represent condensate gas and the white areas represent the precipitated condensate oil.

At the initial pressure of 30 MPa, there are no white areas in the image, indicating that the chip is fully saturated with condensate gas, and no condensate oil has precipitated.

When the pressure of the low condensate oil content gas depletes to 19.16 MPa, condensate oil first appears in the corners and attaches to the pore walls, forming an oil film. Condensate oil first accumulates in the dead-end pores, as indicated by the arrows in Figure 6b.

When the pressure depletes from 19.16 to 14.08 MPa, the amount of precipitated condensate oil significantly increases and accumulates in two large pores, showing an overall increasing trend in condensate oil, as indicated by the arrows in Figure 6b–d.

When the pressure depletes from 14.08 to 8.24 MPa, a large amount of condensate oil is carried out of the pores by the condensate gas from the two large pores, and the condensate oil in the remaining corners is gradually evaporated, showing an overall decreasing trend in condensate oil, as indicated by the arrows from Figure 6d–f.

Figure 7 is an excerpt showing a large pore located in the main flow channel during the microfluidic depletion process of low condensate oil content gas.

As the pressure depletes from 30 to 19.16 MPa, condensate oil first attaches to the large pore walls in the form of an oil film, as indicated by the arrow in Figure 7b.

When the pressure depletes from 19.16 to 14.08 MPa, the condensate oil tends to form a continuous film on the pore walls rather than forming isolated droplets in the middle of the pores, as indicated by the arrow in Figure 7c.

As the pressure continues to decrease, precipitated condensate oil gradually accumulates in the large pore, occupying a portion of the large pore space. Because this large pore is located in the main flow channel, this type of condensate oil accumulation can significantly damage the permeability of the entire pore structure, as indicated by the arrow in Figure 7d.

During the depletion process from 14.08 to 8.24 MPa, the condensate oil in the main large pore significantly decreases. The primary reasons for this decrease are that the condensate oil in the large pores is carried out of the pore structure and is also evaporated. Ultimately, only a layer of oil film remains attached to the pore walls, forming residual oil, as indicated by the arrow in Figure 7f.

Figure 8 shows a pore that is not located in the main flow channel, excerpted from the microfluidic depletion process of low condensate oil content gas.

As the pressure depletes from 30 to 19.16 MPa, the curvature radius at the corners of this pore is relatively small, and the capillary force is larger, making it easier for the liquid phase to form in these corners, as indicated by the arrow in Figure 8b.

When the pressure depletes from 19.16 to 14.08 MPa, the condensate oil in this pore continuously accumulates from areas with smaller pore radii to areas with larger pore radii. Due to the poor connectivity in this region, the liquid phase is difficult to flow and gather, forming oil films or oil droplets in multiple corners, as indicated by the arrow in Figure 8d. Because this pore is not located in the main flow channel, it is difficult for this type of condensate oil to participate in the flow and thus causes less damage to the permeability of the entire pore structure.

When the pressure depletes from 14.08 to 8.24 MPa, the condensate oil is continuously evaporated, leading to a continuous decrease in oil volume. Ultimately, residual oil is formed in the dead-end pore, as indicated by the arrow in Figure 8f.

3.1.2. Comparison of Retrograde Condensation Phenomena in PVT Cells and Porous Media. As shown in Figure 9, the temperature for both the PVT cell and porous media experiments was 70 °C. However, the porous media had a minimum average pore size of 20 μm and a maximum pore size of 330 μm, while the inner diameter of the PVT cell was 3.15 cm. Compared to the PVT cell, this type of porous medium not only has smaller pore sizes but also includes complex flow channels.

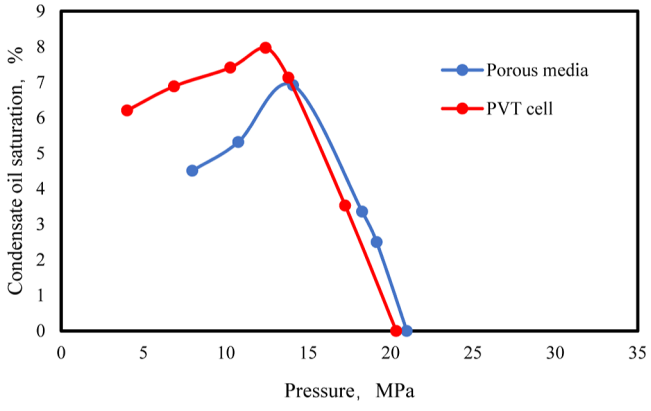

Figure 9. Retrograde condensate volume versus pressure relationship curve during depletion.

https://doi.org/10.1021/acsomega.4c06866
ACS Omega 2024, 9, 43850−43863

Therefore, the experimental results from these porous media can better represent the actual conditions of the real reservoir.

In this set of experiments, during the depletion process in porous media, the dew point pressure of the low-condensate-oil-content gas is 20.98 MPa, which is slightly higher than the dew point pressure of the condensate gas in the PVT cell, which is 20.34 MPa. This set of experiments indicates that during the depletion process in porous media the internal condensate oil saturation trends are consistent with those in the PVT cell. Specifically, during the depletion process, the condensate oil saturation rapidly increases and then slowly decreases. However, the reduction in condensate oil saturation in the PVT cell is less significant than that in the porous media. The reasons are as follows: during the rapid increase stage of condensate oil saturation, the decrease in pressure causes continuous precipitation and aggregation of condensate oil until the maximum condensate oil saturation is reached. In the slow decrease stage, there is no direct outflow of condensate oil in the PVT cell. The reduction in condensate oil is mainly due to the retrograde evaporation effect, where the intermediate and heavy components in the equilibrium gas phase become increasingly scarce. To achieve a phase equilibrium, the corresponding light components in the liquid phase redistribute into the gas phase, thereby reducing the condensate oil volume.

In porous media, the reduction in condensate oil is influenced by two main factors: first, the retrograde evaporation effect and second, the condensate oil is directly carried out of the porous media by the condensate gas. Therefore, the condensate oil saturation in porous media is lower than that in the PVT cell.

In porous media, the precipitated condensate oil is directly carried out by the condensate gas flow, while in the PVT cell, the precipitated condensate oil is mainly influenced by evaporation. Once the oil phase formed in the PVT cell, it could not leave the system with a gas flow. Most of the oil droplets sink to the bottom of the PVT cell. This results in the condensate oil recovery in porous media being much higher than that in the PVT cell, as shown in Figure 10.

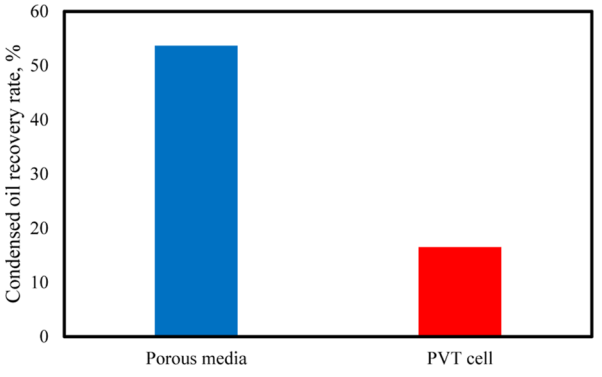

Figure 10. Comparison of condensate oil recovery rates during depletion for low condensate oil content gas.

3.2. Microscopic Depletion Experiment of High Condensate Oil Content Condensate Gas.

3.2.1. Visualization Characterization of Microscopic Occurrence. The entire microscale depletion experiment for a high condensate oil content gas is shown in Figure 11, where the gray areas represent condensate gas and the small white areas represent the precipitated condensate oil.

At the initial pressure of 30 MPa, there are no white areas in the image, indicating that the chip is fully saturated with condensate gas and no condensate oil precipitated, as shown in Figure 11a.

When the pressure depletes to 20.77 MPa, due to the high condensate oil content, the initial precipitation of oil results in large amounts of condensate oil accumulating in corners or dead ends, rather than just attaching to the pore walls as oil films, as indicated by the arrow in Figure 11b.

As the pressure further depletes from 20.77 to 13.53 MPa, the decrease in pressure causes more heavy hydrocarbons to precipitate into liquid condensate oil, showing an overall increasing trend in condensate oil, as shown in Figure 11b–d. At this pressure, the excessive accumulation of condensate oil in the porous media leads to the complete blockage of some main flow channels, significantly damaging the permeability of the porous media, as indicated by the arrow in Figure 11d.

From 13.53 to 7.69 MPa, a large amount of condensate oil is carried out of the porous media by the condensate gas and the effect of retrograde evaporation, resulting in a gradual decrease in condensate oil, as shown in Figure 11d–f. Due to the high condensate oil content, a significant amount of condensate oil remains in the porous media, unable to be evaporated or carried out by the condensate gas flow, eventually forming a considerable amount of residual oil, as indicated by the arrow in Figure 11f.

Figure 12 shows a section of a throat located in the main flow channel, excerpted from the microfluidic depletion process of a high condensate oil content gas.

When the pressure depletes to 20.77 MPa, due to the smaller curvature radius at the corners and the larger capillary force, only two corners precipitated condensate oil droplets, and there is no accumulation of condensate oil in the rest of this pore segment, as shown in Figure 12b.

As the pressure further depletes from 20.77 to 13.53 MPa, the continuous pressure decrease causes more condensate oil to precipitate, completely filling this throat segment with condensate oil and showing a tendency to flow into adjacent pores, as indicated by the arrow in Figure 12d. This causes partial blockage of the flow space in the adjacent pores. The accumulation of condensate oil results in the complete blockage of the throat in the main flow channel, preventing subsequent fluids from passing through and redirecting the flow to other pores. This type of blockage significantly damages the permeability of the entire porous media.

When the pressure depletes from 13.53 to 7.69 MPa, the condensate oil in this throat segment significantly decreases. The main reason for this reduction is the higher flow rate in the main flow channel, which causes gas and liquid to flow more rapidly. The high flow rate carries away the precipitated condensate oil, preventing it from staying and accumulating for a long time. Ultimately, only two corners retain condensate oil droplets, forming residual oil in the corners, as shown in Figure 12f.

Figure 13 shows a section of a dead-end pore, excerpted from the microfluidic depletion process of high condensate oil content gas.

As the pressure depletes from 30 to 20.77 MPa, the smaller curvature radius and larger capillary force in the dead-end promote the precipitation and accumulation of condensate oil. Therefore, condensate oil appears in the form of a plug at this dead-end, with condensate oil at both ends trapping the condensate gas in the dead-end, making it difficult for the condensate gas to flow, as indicated by the arrow in Figure 13b.

https://doi.org/10.1021/acsomega.4c06866
ACS Omega 2024, 9, 43850−43863

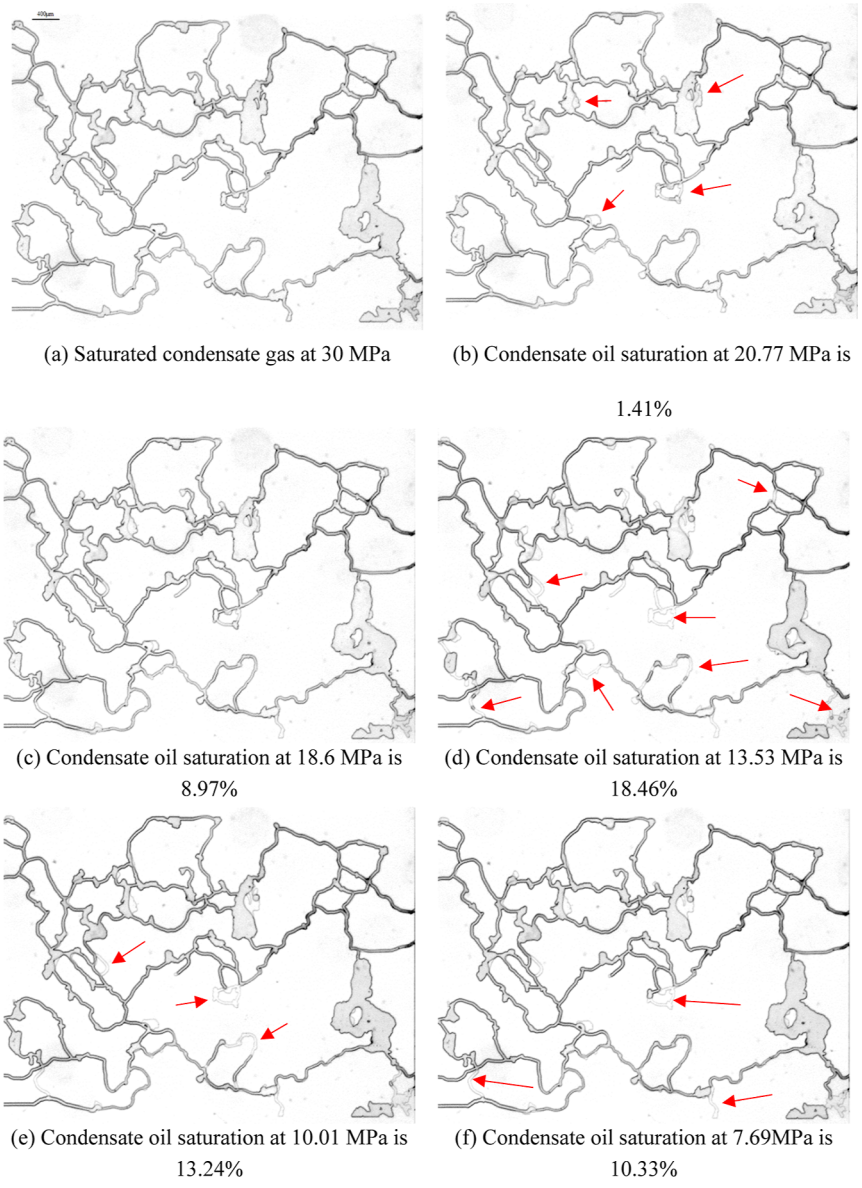

Figure 11. Microscale depletion experiment images of high condensate oil content gas.

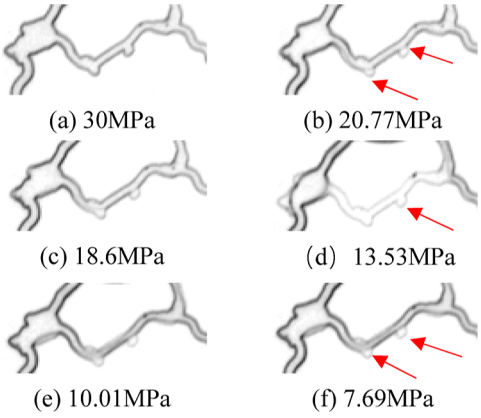

Figure 12. Condensate oil phase change in the throat of the main flow channel during depletion.

When the pressure further depletes from 20.77 to 13.53 MPa, the inability of the dead-end pore to participate in flow leads to continuous precipitation and accumulation of condensate oil until the dead-end pore is filled, as indicated by the arrow in Figure 13d. Because the dead-end pore hardly participates in the flow, this type of condensate oil accumulation has a minimal impact on the permeability of the porous media.

From 13.53 to 7.69 MPa, the nonflowing condensate oil in the dead-end pore gradually decreases, with evaporation playing a major role at this stage. Ultimately, condensate oil forms droplet-shaped residual oil in the dead-end, as indicated by the arrow in Figure 13f.

3.2.2. Comparison of Retrograde Condensation Phenomena in PVT Cells and Porous Media. After processing the original experimental images and performing grayscale analysis, condensate oil saturation within the microfluidic chip during depletion is obtained, as shown in Figure 14.

This experiment shows that during the depletion process in porous media, the dew point of condensate gas with a high condensate oil content in porous media (21.42 MPa) is higher than that in the PVT cell (21.03 MPa). The specific reason is that porous media have a larger specific surface area, which has a

https://doi.org/10.1021/acsomega.4c06866
ACS Omega 2024, 9, 43850−43863

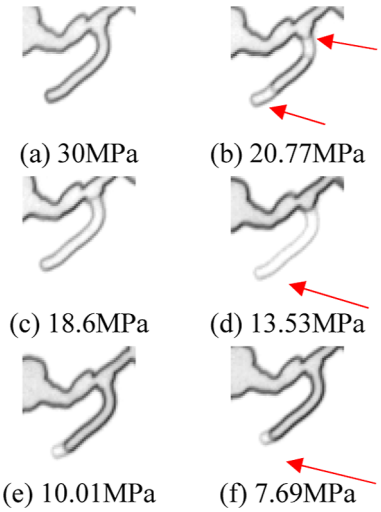

Figure 13. Condensate oil phase change in a dead-end pore during depletion.

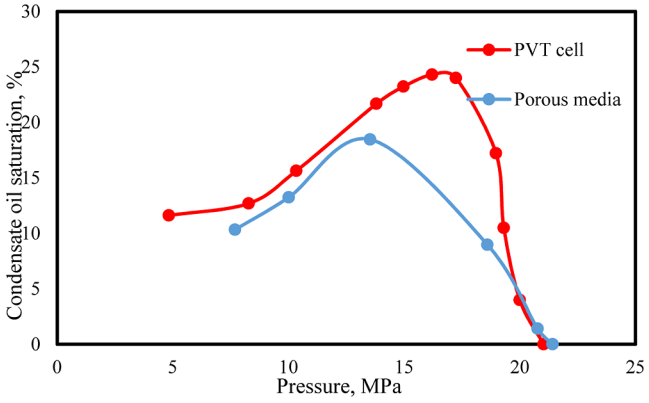

Figure 14. Retrograde condensate volume versus pressure relationship curve during depletion.

stronger adsorption effect on heavy hydrocarbon components, accelerating the precipitation of condensate oil. The capillary condensation effect also impacts the retrograde condensation process.[27,28] Therefore, the dew point of the condensate gas in porous media is slightly higher than that in the PVT cell.

The internal condensate oil saturation trends are consistent with those in the PVT cell. Specifically, during the depletion process, the condensate oil saturation rapidly increases and then slowly decreases. However, the reduction in condensate oil saturation in the PVT cell is less significant than that in porous media.

Combining the patterns observed in Figures 9 and 14, it can be seen that the condensate oil saturation in the early stages of depletion in porous media is higher than that in the PVT cell, while in the mid-to-late stages of depletion, the condensate oil saturation in porous media is lower than that in the PVT cell.

The specific reasons for this are as follows: The pore structure in porous media is complex, with storage space composed of numerous channels, leading to a much larger total surface area compared to a flat surface. As a result, porous media exhibit strong adsorption properties and exert a greater attraction on heavier hydrocarbons, making them more likely to adsorb onto the pore walls. Additionally, the presence of capillary condensation effects in the pores of porous media causes the adsorption film in the pores to act as a nucleation site, filling smaller pores with condensate oil first. These effects are not present in the PVT cell. Therefore, the presence of porous media in the early stages of depletion facilitates the precipitation of condensate oil.[29,30]

In the middle-to-late stages of depletion, due to the complex flow paths in porous media and the differences in mobility between gas and liquid phases, the liquid phase is easily displaced from the pores during fluid redistribution, which can lead to a significant reduction in condensate oil saturation. In the PVT cell, the liquid phase is less likely to be carried away by the gas phase with enough equilibrium time, leading to gradual accumulation and deposition of condensate oil at the bottom of the PVT cell during depletion, resulting in a relatively higher condensate oil saturation. Therefore, the condensate oil saturation in the mid-to-late stages of depletion in porous media is lower than that in the PVT cell.

As shown in Figure 15, the condensate oil recovery in porous media is significantly higher than that in the PVT cell. The main

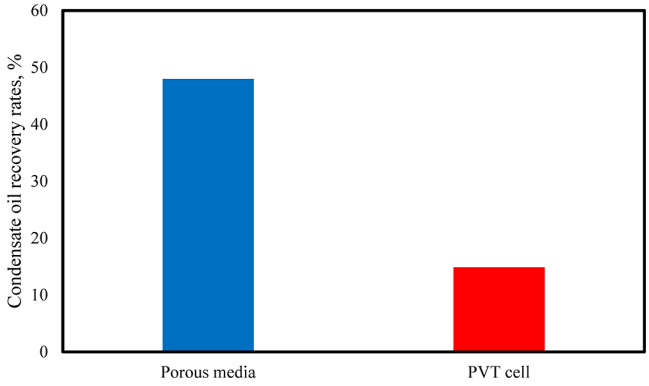

Figure 15. Comparison of condensate oil recovery rates during depletion for high condensate oil content gas.

reason for this phenomenon is that the precipitated condensate oil in porous media is carried out of the porous media structure along with the condensate gas flow. In the PVT cell, the precipitated condensate oil settles at the bottom of the PVT cell due to gravity and cannot flow out. It can only be extracted through evaporation, and the amount of condensate oil extracted this way is far less than the amount carried out in porous media. Therefore, the condensate oil recovery in porous media is much higher than that in the PVT cell.

3.3. Comparison of Condensate Oil Precipitation during Depletion for Different Condensate Oil Content Gases.

The figure in the following section compares the initial oil precipitation state during depletion for condensate gases with different condensate oil contents.

In the depletion process of low condensate oil content gas, after depletion to the dew point pressure, due to the low content of heavy components in the low condensate oil content gas, the condensate oil first appears as point-like oil droplets in a few corners, with no condensate oil precipitation in the remaining pore corners, as indicated by the red arrow in Figure 16a. The condensate oil mainly attaches to the pore walls in the form of oil films or oil droplets in large pores, as indicated by the blue arrow in Figure 16a.

For high condensate oil content gas, after depleting to the dew point pressure due to the high content of heavy components, the condensate oil precipitates in multiple corners, as indicated by the red arrow in Figure 16b. In poorly connected pores, it

https://doi.org/10.1021/acsomega.4c06866
ACS Omega 2024, 9, 43850−43863

(a) Low condensate oil content gas initial (b) High condensate oil content gas initial

Figure 16. Depletion images of two types of condensate gas showing initial oil precipitation for different condensate oil contents.

accumulates to form large patches, completely blocking the flow channels, as indicated by the black arrow in Figure 16b. The condensate oil also aggregates in the large pores, as indicated by the blue arrow in Figure 16b.

The following figure compares the state of maximum condensate oil precipitation during the depletion process for condensate gases with different condensate oil contents.

In the depletion process of low condensate oil content gas, at the point of maximum condensate oil precipitation, the condensate oil is mainly distributed in two large pores, as indicated by the red arrow in Figure 17a. Only a small amount of condensate oil accumulates in a few dead-end pores, as indicated by the blue arrow in Figure 17a. There is also some condensate oil accumulation in a few poorly connected corners, as indicated by the black arrow in Figure 17a. From Figure 17a, it can be concluded that during the depletion process of low condensate oil content gas, the precipitation of condensate oil almost never blocks the throats, thus having a minimal impact on the overall permeability of the porous media.

In the depletion process of high condensate oil content gas, at the point of maximum condensate oil precipitation, a significant amount of condensate oil accumulates in two large pores, as indicated by the red arrow in Figure 17b. The precipitated condensate oil nearly fills every dead-end pore, as indicated by the blue arrow in Figure 17b. Due to the high condensate oil content, the precipitated condensate oil aggregates in a plug-like form, completely filling and blocking some of the pores and throats that need to participate in flow and preventing subsequent fluids from passing through. This has a significant impact on the overall permeability of the porous media, as indicated by the black arrow in Figure 17b.

From the above analysis, it can be concluded that during the depletion process of condensate gas with different condensate oil contents, the form of condensate oil precipitation at different times and the degree and mechanism of blockage in porous media differ significantly. Understanding these blockage mechanisms is of great practical significance for optimizing the development strategies of condensate gas reservoirs and improving the recovery of condensate oil.

4. CONCLUSIONS

This study provides an in-depth examination of the condensate gas depletion process in porous media by using a microfluidic system. We could draw the following conclusions from the excremental results.

1. Due to the adsorption effect and capillary condensation in porous media, the dew point of condensate gas in porous media is slightly higher than the dew point of condensate gas in a PVT cell.
2. The trend of condensate oil saturation variation in porous media are consistent with those observed in PVT cells, with notable differences. Initially, the condensate oil saturation in porous media is higher due to capillary condensation and the presence of larger nucleation sites. However, as depletion progresses, the saturation in porous media decreases more significantly than in PVT cells due to the combined effects of retrograde evaporation and the direct removal of condensate oil by the flowing gas.
3. The condensate oil recovery is significantly higher in porous media than in PVT cells. This is attributed to the flow of condensate oil in the porous media, which is carried out by the condensate gas, unlike in PVT cells where condensate oil tends to settle and is primarily extracted through evaporation.
4. Low condensate oil content gas results in minimal pore blockage and less impact on permeability, while high condensate oil content gas leads to significant pore blockage and substantial permeability reduction.

The limitation of this study is that while considering the complex flow paths of porous media, it is not possible to simultaneously achieve pore sizes at the nanometer scale. Future research could focus on preparing nanometer-scale chips that account for the complex flow paths of porous media to study the phase behavior changes and flow patterns of condensate gas.

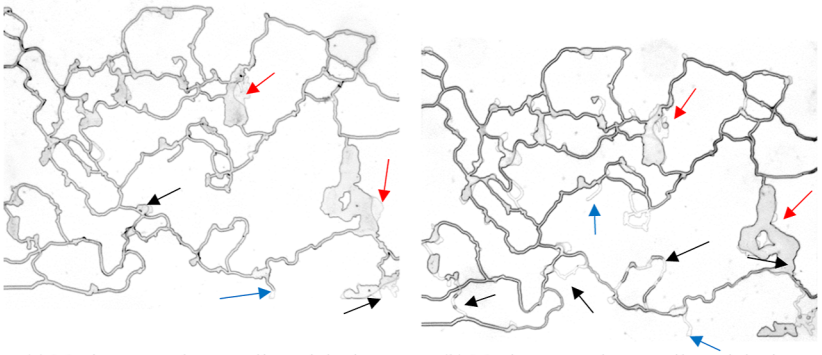

(a) Maximum condensate oil precipitation during depletion for low condensate oil content gas. (b) Maximum condensate oil precipitation during depletion for high condensate oil content gas.

Figure 17. Depletion images at maximum condensate oil saturation for two types of condensate gas with different condensate oil contents.

https://doi.org/10.1021/acsomega.4c06866
ACS Omega 2024, 9, 43850−43863

Additionally, considering the impact of gravity on microscale experiments would also be highly valuable.

AUTHOR INFORMATION

Corresponding Authors

Ping Guo − *National Key Laboratory of Oil and Gas Reservoir Geology and Exploitation, Southwest Petroleum University, Chengdu 610500, China;* orcid.org/0000-0003-2944-3123; Email: guopingswpi@vip.sina.com

Shuoshi Wang − *National Key Laboratory of Oil and Gas Reservoir Geology and Exploitation, Southwest Petroleum University, Chengdu 610500, China;* orcid.org/0000-0003-2442-9824; Email: shuoshi.wang@swpu.edu.cn

Authors

Hengjie Liao − *Shanghai Branch of CNOOC Limited, Shanghai 200335, China*

Xianke He − *Shanghai Branch of CNOOC Limited, Shanghai 200335, China*

Yuansheng Li − *Shanghai Branch of CNOOC Limited, Shanghai 200335, China*

Zhehao Jiang − *Shanghai Branch of CNOOC Limited, Shanghai 200335, China*

Limiao Wang − *National Key Laboratory of Oil and Gas Reservoir Geology and Exploitation, Southwest Petroleum University, Chengdu 610500, China;* orcid.org/0009-0007-1546-2119

Ruifeng Xu − *National Key Laboratory of Oil and Gas Reservoir Geology and Exploitation, Southwest Petroleum University, Chengdu 610500, China;* orcid.org/0009-0005-4384-5796

Hanmin Tu − *National Key Laboratory of Oil and Gas Reservoir Geology and Exploitation, Southwest Petroleum University, Chengdu 610500, China;* orcid.org/0009-0002-8515-3948

Complete contact information is available at: https://pubs.acs.org/10.1021/acsomega.4c06866

Notes

The authors declare no competing financial interest.

ACKNOWLEDGMENTS

This research work was partly supported by the Sichuan Natural Science Foundation, China (grant number 2022NSFSC1029).

REFERENCES

(1) Chunsheng, W.; Lei, Z.; Liangye, S. Well Testing Technology and Production Dynamics Analysis of Condensate Gas Reservoir. *Chem. Technol. Fuels Oils* **2020**, *56* (3), 411−419.

(2) Guo, P. *Theory and Application of Fluid Phase in Oil and Gas Reservoirs*; Petroleum Industry Press, 2004; p 215.

(3) Condensate, H. U. Y. *Fluid Phase and Seepage Mechanism of Low Permeability Gas Reservoirs*; Science Press, 2010; p 191.

(4) Hosseinzadegan, A.; Mahdiyar, H.; Raoof, A.; Nikooee, E.; Qajar, J. The pore-network modeling of gas-condensate flow: Elucidating the effect of pore morphology, wettability, interfacial tension, and flow rate. *Geoenergy Sci. Eng.* **2023**, *229*, 211937.

(5) Labed, I.; Oyeneyin, B.; Oluyemi, G. Gas-condensate flow modelling for shale reservoirs. *J. Nat. Gas Sci. Eng.* **2018**, *59* (0), 156−167.

(6) Ursin, J. Fluid flow in gas condensate reservoirs: the interplay of forces and their relative strengths. *J. Pet. Sci. Eng.* **2004**, *41* (4), 253−267.

(7) Long, K.; Tang, Y.; He, Y.; Wang, Y.; Qin, J.; Tang, L. Fluid phase behavior during multi-cycle injection and production of underground gas storage based on gas-condensate reservoirs with oil rim. *Geoenergy Sci. Eng.* **2023**, *226*, 211769.

(8) Chen, L.; Luo, J.; Rao, H.; et al. Gas injection in the middle and late stages of condensate reservoir development to enhance oil recovery. *Petrol. Geol. Xinjiang* **2019**, *40* (1), 98−102.

(9) Zhang, J.; Wang, H.; Vandeginste, V.; Miao, H.; Guo, Y.; Ji, Y.; Liu, P.; Peng, Y. Effect of litho-facies on nano-pore structure of continental shale in shuinan formation of Jiaolai Basin. *Geoenergy Sci. Eng.* **2023**, *228*, 212020.

(10) Luo, S.; Chen, F.; Zhou, D.; Nasrabadi, H. Multiscale Pressure/Volume/Temperature Simulation of Decreasing Condensate/ Gas Ratio at Greater than Dewpoint Pressure in Shale Gas-Condensate Reservoirs. *SPE J.* **2021**, *26* (06), 4174−4186.

(11) Sui, S.; Guo, P.; Du, J.; et al. Experimental study of condensate gas exhaustion in hypotonic porous media. *J. Southwest Pet. Univ.* **2010**, *32* (3), 97−100.

(12) Zhang, X.; Tang, L.; Li, B.; et al. Study on phase characteristics of condensate gas reservoirs in Bohai Oilfield. *J. Yangtze Univ.* **2016**, *13* (32), 79−81.

(13) Guo, P.; Wang, J.; Liu, W.; et al. Experimental Study on the Dynamic Performance of Exhaustion Production in Fractured Condensed Gas Reservoirs. *Technol. Oil Drill. Prod.* **2013**, *35* (2), 67−70.

(14) Wang, Z.; Song, W.; Liu, J.; et al. Experimental results of long core displacement in the Lunnan buried hill carbonate reservoir. *Xinjiang Pet. Geol.* **2006**, *27* (1), 68−70.

(15) Zhao, M.; Yue, L. Laboratory study on improving crude oil recovery by miscible flooding. *Fault-Block Oil Gas Field* **1996**, *3* (5), 20−23.

(16) Liu, D.; Zhang, J.; Wang, Y.; et al. Method and application of identifying gas channeling in condensate gas reservoirs with cyclic gas injection. *Nat. Gas Explor. Dev.* **2008**, *31* (4), 27−29.

(17) Chenetal, H. L.; Xu, M.; Guo, Q.; et al. Determination of relative permeability and recovery efficiency in Beihai condensate gas reservoirs. *Foreign Oilfield Eng.* **2000**, *10* (10), 1−8.

(18) Wei, H.; Chengyuan, L.; Zengmin, L.; et al. Constant volume depletion experiment and phase behavior characteristics of condensate gas in tight porous media. *Acta Pet. Sin.* **2019**, *40* (11), 1388−1395.

(19) Li, Q. L. Q.; Li, X. L. X.; Zan, K. Z. K.; Song, Z.; Shi, J.; Wu, K. Experimental Research of Critical Condensate Saturation and Flow Characteristics of Gas Condensate Reservoir. *Pet. Sci. Technol.* **2013**, *31* (13), 1361−1370.

(20) Li, X.; Xiao, K.; Wang, R.; Li, X. Experimental Research on Enhanced Oil Recovery Methods for Gas Injection of Fractured Reservoirs Based on Microfluidic Chips. *ACS Omega* **2022**, *7* (31), 27382−27389.

(21) Bao, B.; Riordon, J.; Mostowfi, F.; Sinton, D. Microfluidic and nanofluidic phase behaviour characterization for industrial CO2, oil and gas. *Lab Chip* **2017**, *17* (16), 2740−2759.

(22) Wang, Z.; Li, X.; Cheng, S.; et al. Influencing factors of condensate gas phase transition in porous media. *Nat. Gas. Ind.* **2006**, *26* (1), 90−92.

(23) Zhu, W.; Liu, X.; Shi, Z.; et al. Study on the micro-flow mechanism of wax deposition in condensate gas-liquid-solid systems. *Acta Pet. Sin.* **2007**, *28* (2), 87−90.

(24) Yang, Q.; Jin, B.; Banerjee, D.; et al. Direct visualization and molecular simulation of dewpoint pressure of a confined fluid in sub-10 nm slit pores. *Fuel* **2019**, *235*, 1216−1223.

(25) Zhong, J.; Riordon, J.; Zandavi, S. H.; Xu, Y.; Persad, A. H.; Mostowfi, F.; Sinton, D. Capillary Condensation in 8 nm Deep Channels. *J. Phys. Chem. Lett.* **2018**, *9* (3), 497−503.

(26) Jing, W.; Zhang, L.; Li, A.; Liu, T.; Cheng, Y.; Sun, H.; Yang, Y.; Zhu, G.; Yao, J.; Zhong, J. Phase Behaviors of Gas Condensate at Pore Scale: Direct Visualization via Microfluidics and In-Situ CT Scanning. *SPE J.* **2024**, *29* (05), 2566−2577.

(27) Du, J.; Li, S.; Sun, L.; et al. Study on the effect of capillary condensation in porous media on the dew point of condensate gas reservoirs. *Nat. Gas. Ind.* **2001**, *21* (3), 56−62.
(28) Tong, M.; Li, X.; Hu, Y.; et al. Effect of porous media on the phase behavior of condensate gas. *J. China Univ. Pet., Ed. Nat. Sci.* **2004**, *28*(56164).
(29) Li, J.; Li, X.; Tong, M.; et al. A new experimental method for gas-liquid phase transition of condensate gas in porous media. *Petrol. Explor. Dev.* **2004**, *31* (4), 101−104.
(30) Igwe, U.; Khishvand, M.; Piri, M. Retrograde condensation in natural porous media: An in situ experimental investigation. *Phys. Fluids* **2022**, *34* (1), 1−23.

https://doi.org/10.1021/acsomega.4c06866
ACS Omega 2024, 9, 43850−43863